The
University
Of
Sheffield.

This is a repository copy of *A turn fault mitigation strategy based on current injection technique for a triple 3-phase PMA SynRM*.

White Rose Research Online URL for this paper:
http://eprints.whiterose.ac.uk/143259/

Version: Accepted Version

White Rose
university consortium
Universities of Leeds, Sheffield & York

eprints@whiterose.ac.uk
https://eprints.whiterose.ac.uk/

A Turn Fault Mitigation Strategy Based on Current Injection Technique for a Triple 3-phase PMA SynRM

Bo Wang, *Member IEEE*, Jiabin Wang, *Senior Member, IEEE*, Antonio Griffo, *Member IEEE,* Lei Huang*, Member IEEE*

Abstract—**A turn-to-turn short circuit fault usually causes excessive fault current because of very low impedance associated with a few fault turns. It should be dealt with promptly to avoid further damages to the machine, especially for a permanent magnet (PM) machine. In order to limit the turn fault current, a novel turn fault mitigation strategy based on current injection technique is investigated for a triple redundant 3x3-phase PM synchronous reluctance machine (PMA SynRM). First, the flux linkage of the faulty phase where the fault turns are located is estimated considering the influence of PM and currents in the healthy and faulty 3-phase sets. This flux linkage, including that of the fault turns, is subsequently reduced by injecting specific currents to the faulty 3-phase set, leading to much smaller fault current. The proposed current injection method does not affect the operation of the healthy 3-phase sets which continue to produce torque. The effectiveness of the proposed method is validated by extensive finite element (FE) simulation and experimental tests on a prototype 3x3-phase fault tolerant PMA SynRM drive.**

Index Terms—**Fault tolerant, fault mitigation, magneto-motive force, turn fault, fault location, current injection.**

I. INTRODUCTION

A turn-to-turn short circuit fault, referred to as turn fault, is known as one of the worst fault cases in electrical machine drives. It usually involves only a few turns due to insulation breakdown and results in very low impedance for the short circuit loop. As a result, excessive current will be induced in the fault path and jeopardize the whole machine drives [1, 2]. According to the survey in [3-6], the stator turn fault accounts for about 21% of total failures in the machine drives. The turn fault is more challenging for PM machines because the PM field cannot be turned off in the event of turn fault. Even if the armature windings are de-excited, the PM field can still induce large current in the fault turns. Therefore, the turn fault should be detected and mitigated timely [5], especially for a PM machine.

Various fault detection algorithms have been investigated based on monitoring parameter changes [7], harmonic current [8] and PWM ripple current [9]. Further, the fault detection techniques described in [10, 11] provide

a means to identify the phase location of the fault turns. Turn fault in a multiple 3-phase machine cannot be simply tolerated by switching off the 3-phase inverter associated with the faulty winding since the currents in the healthy 3-phase windings and rotor PM can still induce current in the fault turns. In [2], terminal short circuit (TSC) was applied on the fault phase with a turn fault. Reactive current was induced in the fault phase to reduce the flux linkage in the fault turns and the resultant fault current. However, the study in [12] showed that this approach was only effective for a small wire wound machine and was not suitable for a bar wound machine. Therefore, an optimized current at 90° lagging the back electromotive (emf) was injected to the fault phase to limit the fault current. In [13], a magnet flux nullifying control was developed for a 3-phase interior PM machine (IPM) following a short circuit fault either in the inverter or an entire phase winding by employing open-end winding drives. It was demonstrated that the fault current was reduced to zero by injecting proper current to the healthy phases. In [14], the fault current was reduced for a three-phase PM machine by activating field weakening before the base speed. The voltage of the fault turns is reduced by increasing negative *d*-axis current. However, the effect of the fault current reduction is quite limited and it is conflicted with the output torque. In addition, the machine has to operate at low speed. In [15], three-phase current injection was used to mitigate turn fault in a PM aircraft starter/generator. It loses its torque capability after the turn fault. The conflict between the fault current and output torque is mainly due to the limited degree of freedom for a three-phase machine.
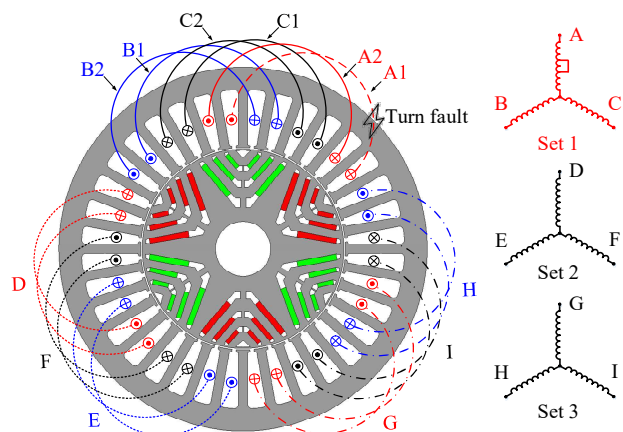
Fig. 1. Triple 3-phase PMA SynRM with segregated windings.

B. Wang and L. Huang are with the School of Electrical Engineering, Southeast University, Nanjing, 210096, China (Email: b.wang@seu.edu.cn, huanglei@seu.edu.cn).

J. Wang and A. Griffo are with the Department of Electronic and Electrical Engineering, University of Sheffield, Sheffield S1 4DE, U.K (Email: j.b.wang@sheffield.ac.uk, a.griffo@sheffield.ac.uk).

In [16], a triple redundant 3x3-phase PMA SynRM machine was proposed as shown in Fig. 1. The conventional overlapped windings were divided into three sets of separate 3-phase windings, resulting in physical and thermal isolation. Each 3-phase set was driven by a standard 3-phase inverter to achieve electrical isolation. Owing to the segregated windings and independent drives, the machine was able to cope with open circuit and short circuit faults as well as uncontrolled generation, etc. [17, 18]. Further a turn fault can be mitigated by application of TSC to the fault 3-phase set. However, the resultant turn fault current differs depending on fault location in the coils [16, 19]. In the worst case, the turn fault current reaches 3.2pu. It would be desirable if the fault current can be reduced further.

This paper aims to develop a mitigation strategy based on current injection to reduce the turn fault current without compromising torque for the triple 3x3-phase PMA SynRM. The flux linkage of the faulted phase, where the fault turns are located, is estimated accounting to the influence of the rotor PM, the currents in the healthy 3-phase sets and the fault set. And no precise information on the number of fault turns and the fault location in sub-coils and slots is required. In order to minimize the flux linkage of the fault turns, specific currents are injected to the fault 3-phase set while the currents in the healthy sets are not affected for continuous torque output. The injected currents are estimated by two linear equations which are independent of the rotor position. The proposed method is validated by extensive finite element (FE) simulations and experimental tests on a 35kW prototype. It is demonstrated that the fault current is effectively reduced compared to the conventional TSC method while the torque is not compromised.

II. PROPOSED CURRENT INJECTION TECHNIQUE

The machine under consideration is a 36-slot 6-pole PMA SynRM whose specifications are listed in Table I. The gamma angle refers to the optimal current vector angle with respect to the q-axis for maximum torque per ampere (MTPA) operation. The N denotes the number of turns for the coils as A1, A2…C2. A turn fault is assumed to take place in set ABC while the sets DEF and GHI are healthy, also named as set 1, 2 and 3, respectively. After a turn fault, TSC can be applied to the faulty 3-phase set to limit the fault current. It has been shown in [15] that in motoring mode, the turn fault current is the highest if the fault occurs in coil B2, whilst in generating mode it is the highest in coil A1. The highest fault current is 3.2pu.

Table I
SPECIFICATIONS OF THE MACHINE

Specification	Symbol	Value
Base speed	n_b	4000 rpm
Maximum speed	n_m	19200 rpm
Rated power	P_r	35 kW
Rated current and gamma angle	I_{rated}	120 A(51°)
Nominal DC link voltage	V_{dc}	270 V
Number of turns in each coil	N	8
Number of faulty turns	N_f	1
d-axis inductance (one 3-phase set)	L_d	0.37 mH
q-axis inductance (one 3-phase set)	L_q	1.3 mH
Constant k	k	0.38e-3

To minimize the fault impact, the flux linkage of the fault turns should be reduced as small as possible so that the fault current can be effectively limited. In the triple redundant 3x3-phase machine, it has more degrees of freedom in the causes of flux linkage than a conventional 3-phase machine. Thus, specific currents can be injected to the fault set to minimize the flux linkage of the fault turns while the remaining healthy sets can continue operation to produce torque.

Due to the mutual coupling between the healthy sets and fault set, it is not possible to nullify all three phases' flux linkages of the fault set. However, only the flux linkage of the fault phase where the turn fault occurs needs to be minimized. Based on the techniques described in [9-11], it is possible to identify the fault phase while the sub-coil location of the fault turns may still be unknown if the phase winding contains more than one coil. For the machine with distributed windings, coils of the same phase are usually placed within 60° phase belt. For example, the machine under consideration has two coils connected in series and they are displaced by 30° with respect to each other as shown in Fig. 2. The phase axis is 15° with respect to the two sub-coils. Thus, if the flux linkage of the fault phase is limited to zero, the flux linkage of the two sub-coils will also be very low, leading to small fault current.

To derive the injected currents, the flux linkage of the fault phase is first analyzed. As shown in Fig. 1, the flux linkage of the fault phase is contributed by three sources, namely, the rotor PM, the currents in the healthy 3-phase sets, and the currents in the fault set. The flux linkage of the fault phase due to the three sources will be analyzed separately, assuming that they can be linearly superimposed. While this condition is generally not true for an IPM machine in saturated condition, it will be shown that the injected currents render the fault 3-phase region unsaturated and the principle of superposition is valid.
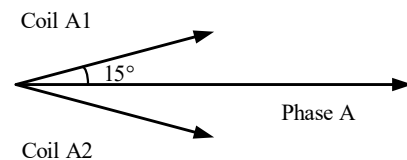

Fig. 2. Phasors of the sub-coils in phase A.

A. Flux Linkage by Rotor PM

First, the flux linkage produced by the rotor PM is analyzed. The magnets on the rotor produce symmetrical flux linkages in ABC phases of the fault set given by (1) when high order harmonics are neglected.

$$\psi_{mA} = \psi_m \cos(p\omega t)$$
$$\psi_{mB} = \psi_m \cos(p\omega t - 120°) \qquad (1)$$
$$\psi_{mC} = \psi_m \cos(p\omega t + 120°)$$

where ψ_m is the magnitude of the PM flux linkage of each phase, ω denotes the mechanical speed of the machine, and p is the number of pole-pairs.

B. Flux Linkage by the Currents in Healthy Sets

Unlike the fault tolerant machines in [20, 21] where mutual magnetic coupling between phases is negligible, the three 3-phase sets of the PMA SynRM are mutually

coupled [22]. The coupling effect can be quantified by analyzing the magneto-motive force (MMF) distribution using the concept of turn function and winding function.

Turn function represents the distribution of winding turns over a defined region in airgap. More details about the winding function can be found in [23]. First, the turn functions of the 6 coils in set ABC are illustrated in Fig. 3 according to the coil displacement over the whole airgap. N is the number of turns of each coil as given in Table I. It should be noted that the turn functions of phase C are negative due to the reversed go-return polarity relative to those in phases A and B as shown in Fig. 1. The turn functions of the coils in healthy sets DEF and GHI can be obtained by 120° and 240° phase shift, respectively, also shown in Fig. 3.
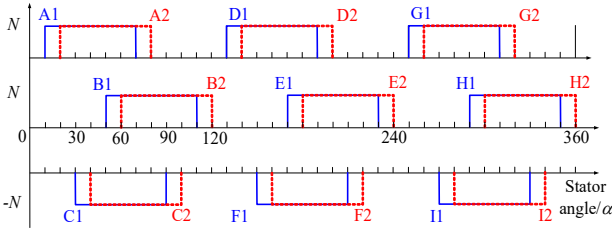

Fig. 3. Turn functions of the coils in sets ABC, DEF and GHI.
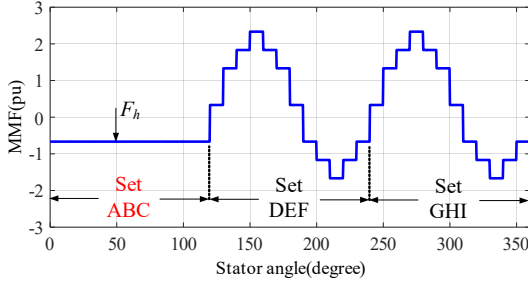

Fig. 4. MMF produced by the healthy sets currents.

The fundamental component of the MMF in a rotary machine rotates synchronously with the rotor and its interaction with the PM field produces electromagnetic torque. The MMF distribution produced by the currents in the healthy sets DEF and GHI can be calculated by multiplying the winding function of the coils with relevant phase currents as described in [23-25] and it is shown in Fig. 4, where the ampere-turn of each coil with the rated current is denoted as 1pu. The detailed derivation can be found in [22]. It should be noted that Fig. 4 only shows the MMF for a given time constant. Since the MMF is related to the currents, the current angle alters the phase angle between the MMF vector and d-axis, and hence the resultant torque. The current angle in dq frame can be adjusted by varying i_d and i_q.

In Fig. 4, the MMF over (0°~120°) region is associated with the fault set ABC. It is observed that only an MMF offset component exists since the MMF produced by the currents in set ABC are not considered at this stage. The MMF offset component F_h in this region is induced by the currents in the healthy sets which can be calculated by (2).

$$F_h = -\frac{1}{3}(i_D + i_E - i_F) - \frac{1}{3}(i_G + i_H - i_I) \qquad (2)$$

where i_D, i_E,.. i_I are the phase currents which can be expressed in terms of the dq currents (i_{dh}, i_{qh}) in (3).

$$i_D = i_G = i_{dh}\cos(p\omega t) - i_{qh}\sin(p\omega t) \qquad (3)$$
$$i_E = i_H = i_{dh}\cos(p\omega t - 120°) - i_{qh}\sin(p\omega t - 120°)$$
$$i_F = i_I = i_{dh}\cos(p\omega t + 120°) - i_{qh}\sin(p\omega t + 120°)$$

Substituting (3) into (2) results in (4):

$$F_h = -\frac{4}{3}(i_{dh}\cos(p\omega t - 60°) - i_{qh}\sin(p\omega t - 60°))$$
$$(4)$$

The MMF in the (120°~240°) and (240°~360°) regions occupied by the healthy sets DEF and GHI consists of a symmetrical AC component and an offset component. The symmetrical component is determined by the healthy currents (i_{dh}, i_{qh}), while the MMF offset component can be calculated similarly.

The resultant flux linkages in the fault 3-phase set due to the currents in the two healthy 3-phase sets are proportional to the MMF offset component F_h. They are given by (5).

$$\psi_{FhA} = kF_h$$
$$\psi_{FhB} = kF_h \qquad (5)$$
$$\psi_{FhC} = -kF_h$$

The k is the proportional constant which represents the coefficient of the flux linkage induced by the MMF offset component. Since the coils are full-pitched and F_h is constant over the ABC set region, the k is independent with rotor position according to [26]. It can be obtained via FE computation by injecting specific MMF offset component over the fault set region. It is possible to predict the constant k analytically for a simple rotor configuration. However, for the rotor with three magnet layers, FE computation is more practical since the FE model is already available. The value of the constant k has been given in Table I. Note that the induced flux linkage of phase C is negative which is due to the reversed turn function relative to those of phases A and B as shown in Fig. 3.

C. Flux Linkage by the Currents in Fault Set

Assuming specific currents (i_{df}, i_{qf}) are injected in the fault set to counteract the flux linkages caused by the PM and healthy set currents in the fault phase, the induced flux linkage can also be calculated by the MMF approach.

The MMF caused by the injected currents (i_{df}, i_{qf}) in ABC set is plotted in Fig. 5 [22]. It is seen that the injected currents produce a symmetrical AC component and an MMF offset component in the fault set region while they give only rise to an MMF offset component over the healthy sets region. The MMF in the fault set region can be decomposed to an AC component and an offset component as shown in Fig. 6.
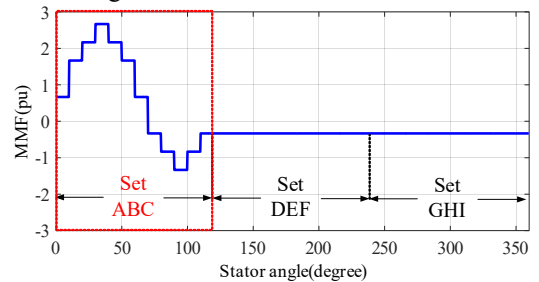

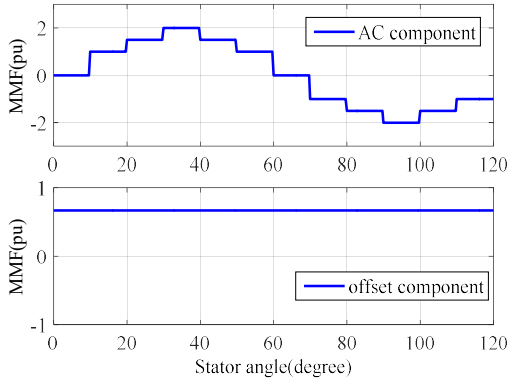Fig. 5. MMF produced by the fault set currents.

Fig. 6. MMF AC and offset component in the fault set.

According to [22], the AC component is the same as the healthy condition when all three sets are excited with (i_{df}, i_{qf}). Hence, the flux linkages induced by the MMF AC component can be calculated by the dq axis inductance (L_d, L_q) in (6), which are further transformed to the phase quantities in (7).

$$\psi_{ACfd} = L_d i_{df}$$
$$\psi_{ACfq} = L_q i_{qf} \tag{6}$$
$$\psi_{ACfA} = L_d i_{df} \cos(p\omega t) - L_q i_{qf} \sin(p\omega t) \tag{7}$$
$$\psi_{ACfB} = L_d i_{df} \cos(p\omega t - 120°) - L_q i_{qf} \sin(p\omega t - 120°)$$
$$\psi_{ACfC} = L_d i_{df} \cos(p\omega t + 120°) - L_q i_{qf} \sin(p\omega t + 120°)$$

The magnitude of the MMF offset component F_f can be calculated according to the turn functions and phase currents which are given in (8).

$$F_f = \frac{2}{3}(i_A + i_B - i_C)$$
$$= \frac{4}{3}(i_{df} \cos(p\omega t - 60°) - i_{qf} \sin(p\omega t - 60°)) \tag{8}$$

The flux linkages due to the MMF offset component can be calculated similarly and they are expressed in (9).

$$\psi_{FfA} = kF_f$$
$$\psi_{FfB} = kF_f \tag{9}$$
$$\psi_{FfC} = -kF_f$$

Hence, the flux linkages in the fault 3-phase set produced by its own currents are obtained.

D. Total Flux Linkage in Fault Phase

From the foregoing analysis, the flux linkages of the fault phase can be obtained by summing equations (1)(5)(7)(9). Without loss of generality, the fault turns are assumed in coil A1 of phase A. Thus the flux linkage of the fault phase A is expressed in (10).

$$\psi_A = (\psi_m + L_d i_{df}) \cos p\omega t - L_q i_{qf} \sin p\omega t$$
$$+ \frac{4k}{3}(i_{df} - i_{dh}) \cos(p\omega t - 60°)$$
$$- \frac{4k}{3}(i_{qf} - i_{qh}) \sin(p\omega t - 60°)) \tag{10}$$

In order to minimize the turn fault current, the flux linkage of the fault phase should ideally be controlled as zero. This requires that the coefficients associated with $\cos p\omega t$ and $\sin p\omega t$ equal to zero. The above equation can be decomposed to two equations as shown in (11) associating with the $\cos p\omega t$ and $\sin p\omega t$, respectively.

$$(\psi_m + L_d i_{df}) \cos p\omega t + \frac{4k}{3}(i_{df} - i_{dh}) \cos p\omega t \cos 60°$$
$$+ \frac{4k}{3}(i_{qf} - i_{qh}) \cos p\omega t \sin 60° = 0$$
$$-L_q i_{qf} \sin p\omega t + \frac{4k}{3}(i_{df} - i_{dh}) \sin p\omega t \sin 60° \tag{11}$$
$$- \frac{4k}{3}(i_{qf} - i_{qh}) \sin p\omega t \cos 60° = 0$$

Hence, the currents (i_{df}, i_{qf}) to be injected to the fault set can be determined as functions of the healthy sets currents (i_{dh}, i_{qh}) based on the two equations. If the currents (i_{df}, i_{qf}) are injected to the fault 3-phase set, the flux linkages of the fault phase will be close to zero. Consequently, the flux linkage of the fault turns and the resultant fault current will be reduced to a very low level. Thus, the impact of the turn fault, excessive fault current and resultant local hotspot, can be mitigated. It should be noted that the derivation of the injected currents from (11) does not require specific knowledge of the fault location of the sub-coils in the fault phase and the number of fault turns. Hence the technique is applicable to various turn fault scenarios. The proposed current injection method will be examined by FE simulations and experimental tests.

III. SIMULATION STUDY

In this section, the effectiveness of the proposed current injection method is investigated by FE simulations. The mitigation effect is compared with the conventional TSC. The influences of fault location in the sub-coils, slot position and the number of the fault turns on the turn fault current are analyzed with the current injection technique.

In FE simulation, the machine is loaded by ideal current sources. The fault turns in a coil are separated from the other healthy turns as shown in set 1 of Fig. 1. More details are described in [27]. The turn fault is emulated by short circuiting the fault turn directly with zero external impedance. In terms of TSC, the 3-phase terminals of the fault set are short circuited while the fault set windings are loaded by ideal current sources under the proposed current injection mitigation method.

A. Effectiveness of Current Injection

First, the turn fault under current injection control is examined at base speed 4000rpm when the healthy sets DEF and GHI are excited with the rated currents (120A, 51°) in motoring mode. A single turn fault occurring in all 6 different coil locations of set ABC has been investigated. In each case, the injected currents are calculated by (11) and they are fed to the fault set. The injected currents in the fault set and the rated current (120A, 51°) in the healthy sets, along with the resultant rms turn fault currents are all given in Table II. The waveforms of the fault currents are shown in Fig. 7. It is seen that the injected currents are different if the turn fault occurs in different phases and their magnitudes are lower than the rated value. This is because the injected currents aim to reduce the flux linkage of the fault phase only where the fault turns are located. The maximum rms turn fault current which results with the injection technique is 1.72pu when the fault occurs in coil A2. According to the investigation in [16], the maximum

turn fault current with TSC was 3.2pu when the fault took place in coil B2 in motoring mode. Thus, the maximum fault current has been reduced by 45% with the proposed current injection technique. The 1.72pu fault current only involves in one fault turn, the incurred copper loss can be easily accommodated by the machine.
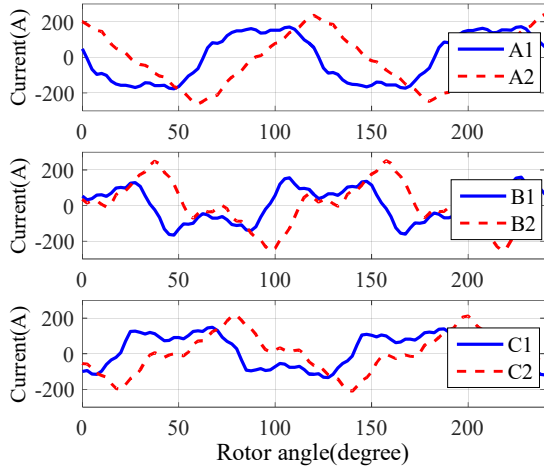

Fig. 7. Single turn fault current waveforms in different coil locations.

Table II
RMS TURN FAULT CURRENTS IN DIFFERENT COIL LOCATIONS

Turn fault coil location	Injected currents	Fault current rms value
A1	(-47.7A, 24.8A)	132A, 1.58pu
A2	(-47.7A, 24.8A)	144A, 1.72pu
B1	(-119A, 19A)	98A, 1.18pu
B2	(-119A, 19A)	127A, 1.52pu
C1	(-85A, 19.7A)	93A, 1.11pu
C2	(-85A, 19.7A)	108A, 1.28pu

As previously mentioned, the saturation effect is not considered in the flux linkage estimation. This is because the injected current to the fault set has a large negative i_d and small i_q as shown in Table II. Therefore, the fault set region operates in deep field weakening region which implies that the main flux path associated with the faulted winding is unsaturated. Hence, the machine can be considered as linear and the error caused by saturation is small.

The main approach of the proposed method is to minimize the flux linkage of the fault turns by injecting specific current to the fault set windings. However, the fault turn flux linkage cannot be completely nullified mainly due to two reasons. First, only the fundamental component is considered while the high order harmonics of the faulted turn flux linkage will also induce short circuit current in the fault turns. Second, the phase angle of the fault turn flux linkage is dependent on the coil location of the fault turns. However, no practical technique exists to detect the fault location to date. Therefore, in the proposed method, it is assumed that the fault turn coincides with the faulted phase axis. This will ensure on average probability of a fault location. The current is injected to minimize the residual flux along the phase axis. Hence if a fault occurs in coil A1, the injected current is 15° leading while it will be 15° lagging in case the fault is in coil A2. Similar is true for the turn fault in phases B and C. Thus, fundamental component of the fault turn flux linkage is not be nullified completely

and fault current still circulates in the fault turns. Nonetheless, it is much lower than that of TSC method. Owing to the above two facts, the injected currents affect the fundamental and high order harmonic flux linkages of the faulted turn in a different manner for different coil locations, and the resultant fault current waveforms shown in Fig. 7 are different.

B. Residual Flux Linkage of the Fault Turns

It has been shown that the proposed current injection technique can reduce the turn fault current further comparing with TSC. The fault current reduction is explained in-depth by comparing the residual flux linkages of the fault turn and fault phase under the two different mitigation strategies. For a single turn fault in coil B2 with rated current excitation in the healthy sets at base speed, the residual phase flux linkages, which results with to the two mitigation measures, have been compared in Fig. 8 and Fig. 9. Under the TSC, the flux linkages of phases ABC are reduced simultaneously. In contrast, when the machine operates in the same condition under the current injection, only the flux linkage of the fault phase B is reduced to a very low level whilst the flux linkages of phases A and C are much higher.

The peak-to-peak residual flux linkages in phase B and fault turn B2f are compared in Table III. It is evident that under the current injection, both the flux linkages of phase B and fault turn B2f are much lower than those with the TSC, and consequently the fault current with the proposed method is lower.
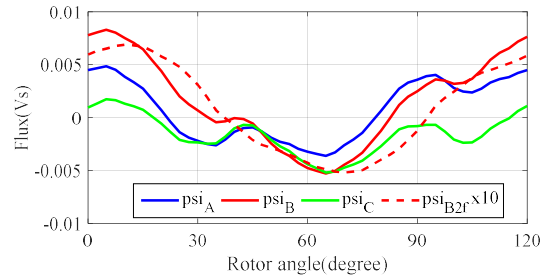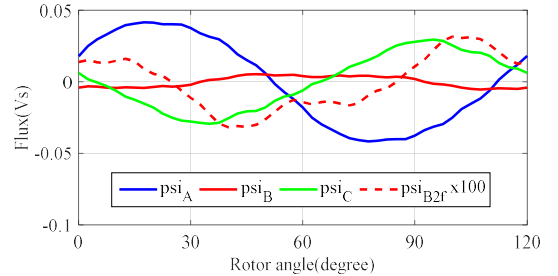

Fig. 8. Residual flux linkages under TSC.

Fig. 9. Residual flux linkages under current injection.

Table III
PEAK-TO-PEAK VALUE OF RESIDUAL FLUX LINKAGE

Residual flux linkage	TSC	Current injection
Fault phase B	1.36e-2 Vs	1.0e-3 Vs
Fault turn B2f	1.2e-3 Vs	0.63e-3 Vs

C. Influence of the Slot Position of Fault Turns

It is essential to analyze the fault current dependency on the slot position of the fault turns as shown in Fig. 10 because the slot leakage inductance has a notable influence on the fault current. The slot leakage inductance is

dependent on the position of the fault turns in the slot. The turn near the slot opening is defined as top turn while the turn close to the stator yoke is defined as bottom turn. The analysis in [21, 28] shows that the turn fault current is the highest if the fault turns are close to the slot opening. Therefore, it is essential to show that the proposed technique is effective for both or any fault locations in a slot between the two.

Hence, a single turn fault which occurs at the top and the bottom in coil B2 slot is analyzed. The same currents are injected to the fault set while the healthy sets are loaded with the rated currents. Fig. 11 compares the resultant turn fault currents when the fault occurs in the two different slot positions. It is shown that the fault turn at the top experiences higher current (1.77pu) than that at the bottom (1.21pu) due to the screening effect [12]. However, the fault current in the top turn is still in the safe thermal range. Thus, the proposed mitigation strategy is effective in the worst turn slot position.
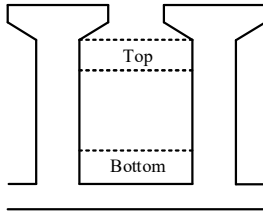

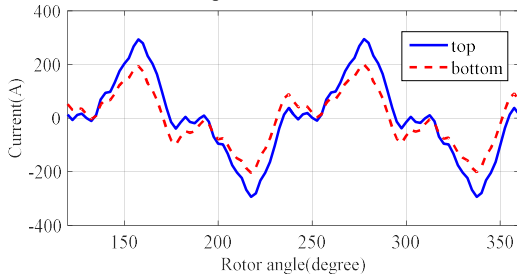Fig. 10. Illustration of the slot position of the fault turn.

Fig. 11. Turn fault currents in different slot position.

D. Influence of the Number of Fault Turns

The fault current is also affected by the number of faulted turns. In case of a turn fault without current injection, the turn fault current decreases as the number of fault turns increases. This is because the inductance of the fault turns is proportional to the square of the number of turns. Meanwhile the flux linkage of the fault turns and the induced voltage are proportional to the number of turns. Therefore, the resultant short circuit current decreases with the increase in the number of faulted turns [2, 23].

However, for the turn fault with current injection, the flux linkage of the fault turns is nullified by assuming that all turns of a fault coils are injected with the current since it is not possible to detect the number of short-circuited turns. The real effect is different for different number of faulted turns. So the turn faults with 1, 2, 4 and 7 short circuited turns in coil B2 are analyzed in FE simulation when the healthy sets are loaded by the rated currents. The same currents are injected to the fault set as given in Table II. The resultant turn fault currents are shown in Fig. 12. It is seen that the fault current decreases as the number of fault turns increases. Thus, the proposed method is effective in

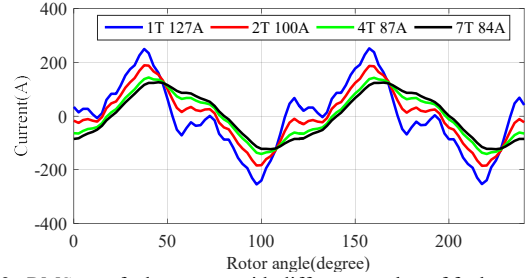reduction of the fault current for different number of fault turns.

Fig. 12. RMS turn fault currents with different number of fault turns.

E. Output Torque

The influence of the proposed current injection on the output torque is assessed. The torques under healthy condition and turn fault condition with different number of fault turns when the two mitigation measures are applied are compared in Fig. 13. Note that all of these fault turns are very close to the slot opening. It is seen that the machine under different turns fault exhibits almost the same torque, as a result, they coincides with each other and some of them are not visible.

The results show that the output torque under current injection method is ~10% higher than that of TSC. The torque is slightly boosted primarily because the injected currents are all with negative i_d and positive i_q as shown in Table II. They will produce positive torque in the fault set region. In the TSC method, only reactive currents flow in the fault set windings, resulting in negative i_d and nearly zero i_q. They produce much less torque.

The torque boost can be explained by analyzing the torque contributions of each set region as shown in Fig. 14, taking one turn fault as an example. It is seen that the healthy sets, viz. set 2 and set 3 produce similar torque under the two mitigation strategies. However, the fault set under current injection contributes higher torque than that of TSC. Hence, the machine with current injection method can provide higher torque.
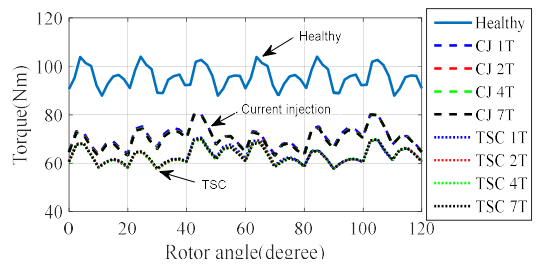

Fig. 13. Output torques under different mitigation strategies considering different fault turns.
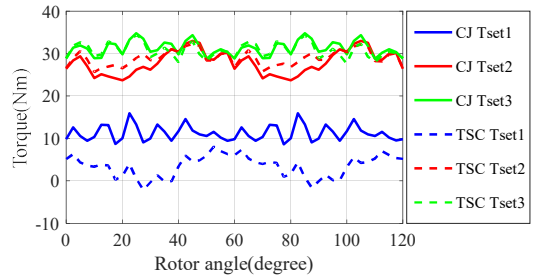

Fig. 14. Torque contribution of different set regions under two mitigation strategies with one turn fault.

In generating mode, the healthy sets windings are operating with negative i_d and negative i_q. The derived injected current in the fault set will be also negative i_d and negative i_q. Consequently, it also produces higher torque (breaking torque) than that of the TSC method.

F. Effectiveness at high speed

It is well known that the fault current increases with speed and will become stable at a relative high speed if with the same load currents. Thus, one turn fault in coil A1 has been simulated in FE at maximum speed 19200rpm. The currents in the healthy sets windings are (60A, 70°). The injected currents in the fault set windings are calculated as (i_{df}: -54.9A, i_{qf}: 3.8A). The simulated turn fault current is shown in Fig. 15. It is found the fault current is lower than the rated value. The reason is because the all three 3-phase sets operate in deep field weakening region, as a result, the machine is not saturated and it can be considered as linear. Consequently, the proposed method can reduce the flux linkage of the fault turn more effectively.
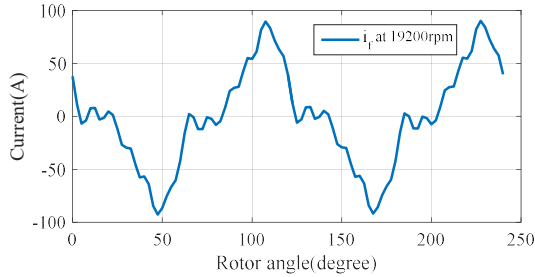

Fig. 15. Simulated turn fault current in coil A1 at 19200rpm.

IV. EXPERIMENTAL TEST

The proposed current injection method has been tested on a triple redundant 3x3-phase PMA SynRM whose specifications are given in Table I. The schematic of the proposed current injection control diagram is shown in Fig. 16. The calculation block provides the current commands for the fault set windings according to the fault phase location and currents feedback from the healthy sets windings based on equation (11). Then the three dq current controllers track the current commands independently. The machine prototype is shown in Fig. 17. As can be seen, the machine windings are separated by the segregated winding configuration. In order to test the turn fault behavior under the proposed current injection technique, two taps for a single turn fault are brought out from coil B2 of set ABC for emulating a single turn short circuit. The taps are connected via thick cables to a high current relay to emulate single turn fault in a controlled manner. The schematic turn fault implementation is shown in Fig. 17(d). The integrated test rig is shown in Fig. 18 where the machine is connected to the dynamometer via an inline torque transducer. The machine is fed by a DSP based 9-phase inverter. Each 3-phase set is controlled by an independent 3-phase inverter which tracks current commands. The DSP sampling frequency and inverter switching frequency are set to 10 kHz.
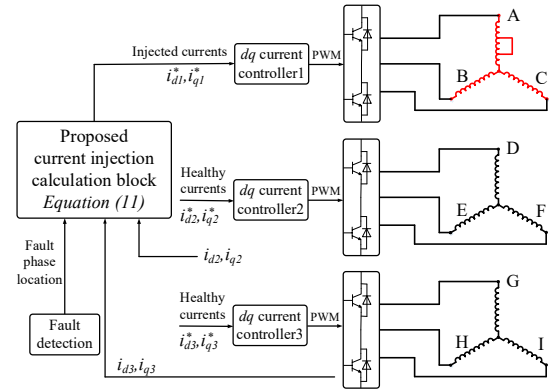

Fig. 16. Schematic of the proposed current injection control diagram.
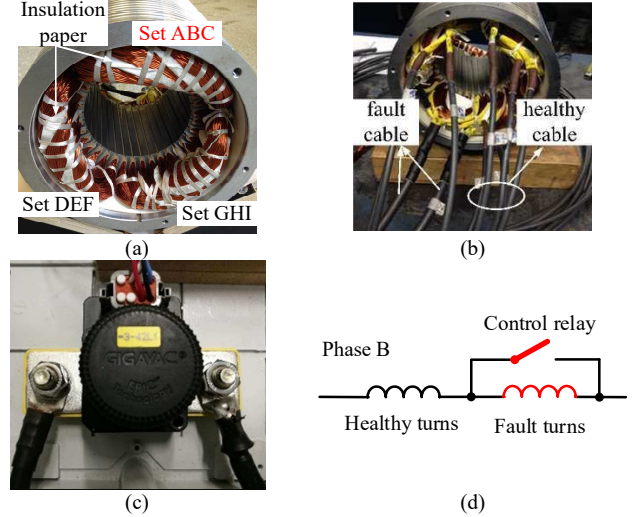

Fig. 17. Triple 3x3-phase PMA SynRM prototype (a) segregated windings (b) cable leads (c) control relay (d) turn fault illustration.
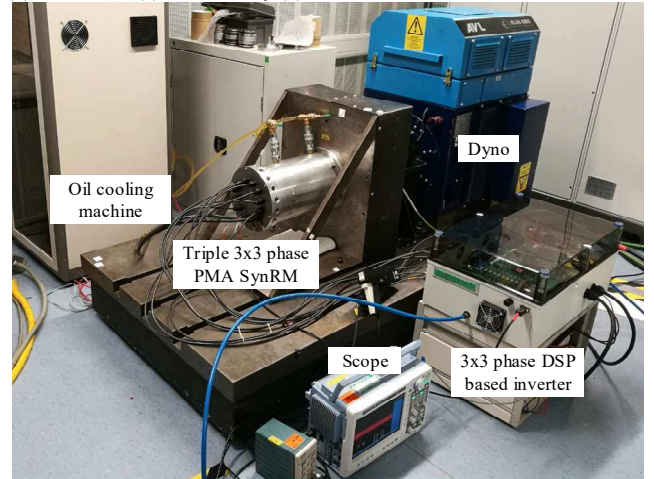

Fig. 18. Test rig of the prototype machine drive.

A. Turn Fault in Coil B2

First, the turn fault in coil B2 is tested under the two mitigation methods, namely, TSC and the proposed current injection method when the healthy sets are loaded with the rated currents 120A at 4000rpm. The resultant turn fault current and phase currents under the two mitigation measures are shown in Fig. 19 and Fig. 20. Under the TSC, the phase currents in the fault set are reactive and they are highly unbalanced due to the mutual coupling with the healthy sets as seen in Fig. 19(a). Consequently, the rms fault current is relatively higher at 166.6A albeit the currents in the healthy sets are well controlled as shown in

Fig. 20(a). When the phase currents of the fault set are controlled by the proposed current injection method, they exhibit a reasonable level of symmetry due to the closed loop current controller while the currents in the healthy sets are also well-controlled as is evident in Fig. 19(b) and Fig. 20(b). Since the flux linkages of the fault phase and the fault turn are minimized by the injected currents, the resultant rms fault current is only 68A, much lower than that of the TSC scheme.
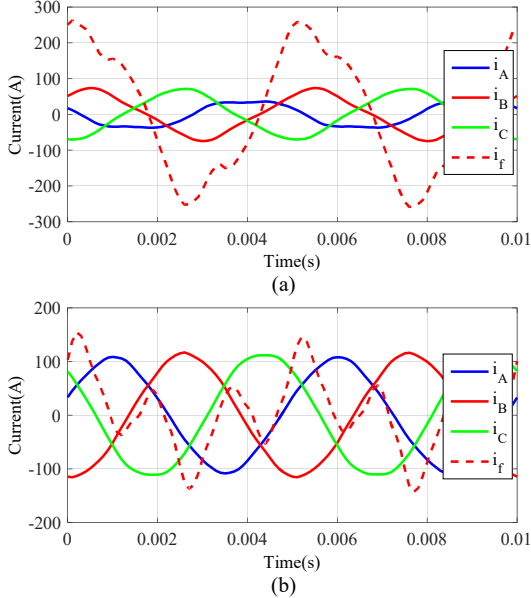

Fig. 19. Fault current and phase currents in set ABC (a) with TSC (b) with current injection.
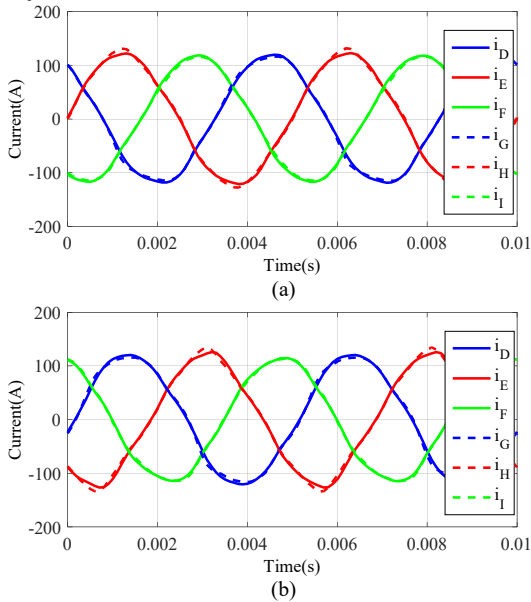

Fig. 20. Phase currents in sets DEF and GHI (a) with TSC (b) with current injection.

It should be noted that due to the limited number of available current probes, the 9 phase currents and fault current are mainly measured by the inverter current sensors and the data are stored in the DSP RAM. Consequently the switching harmonics are not visible due to the limited sampling frequency and anti-alias filtering.

The effectiveness of the proposed method is also validated in a wide operation range by varying the healthy sets currents from 20A to 120A. For the purpose of comparison, the turn fault current without mitigation action

is tested at a low speed 1000rpm since the fault current is excessive at 4000rpm which may cause permanent damage to the machine. It is seen the fault current with no action is about 4 times of the rated value and it will be even larger at higher speed. Thus, effective mitigation method is essential to limit the excessive fault current. The resultant turn fault current under TSC and current injection at 4000rpm are compared in Fig. 21. It is seen the turn fault currents are effectively reduced for the both strategies. And it is the lowest for the proposed current injection method in whole operation range.
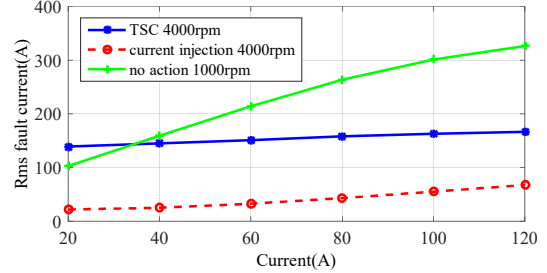

Fig. 21. Rms turn fault current variation with healthy sets currents with turn fault in coil B2 in different operation conditions.

Meanwhile, the torques in healthy condition are compared with those under TSC and current injection method by varying the healthy sets current from 20A to 120A in Fig. 22 and Table IV. It is seen that the output torques under current injection control are always higher than those of TSC when the fault turn is in coil B2. The torque reduction under current injection with 120A current is 20Nm which about quarter of the rated torque. At low current range, the torque under current injection is close to the healthy condition since the injected currents contribute some torque in the fault set region and the overall torque is almost the same.
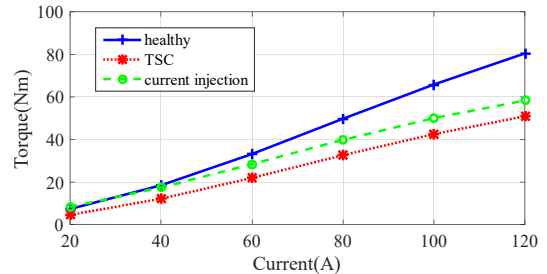

Fig. 22. Variations of torque with the load currents at 4000rpm in different operation conditions.

Table IV
COMPARISON OF THE OUTPUT TORQUES VARIATIONS WITH THE LOAD CURRENTS UNDER DIFFERENT OPERATION CONDITIONS

Load current	Healthy operation	B2 TSC	B2 CJ	A1 TSC	A1 CJ
20 A	7.3 Nm	4.5 Nm	8.3 Nm	4.5 Nm	5 Nm
40 A	18.4 Nm	12.1 Nm	17.4 Nm	12.1 Nm	13 Nm
60 A	33.1 Nm	21.9 Nm	28.4 Nm	21.9 Nm	23.1 Nm
80 A	49.7 Nm	32.6 Nm	39.8 Nm	32.6 Nm	33.5 Nm
100 A	65.7 Nm	42.5 Nm	50 Nm	42.5 Nm	43.1 Nm
120 A	80.4 Nm	50.9 Nm	58.3 Nm	50.8 Nm	51.5 Nm

B. Turn Fault in Coil A1

As shown in Fig. 1, the fault turn is located in coil B2 when the rotor rotates anti-clockwise. However, the equivalent fault location of the fault turn will be in coil A1 if the rotor rotates clockwise. Hence, the turn fault can also

be tested in coil A1 by rotating clockwise. This fault scenario is also tested at 4000rpm while the healthy sets are loaded with 120A currents. Due to the paper length limit, only the current waveforms under the current injection control are shown in Fig. 23. It is seen that the turn fault current is limited effectively and the phase currents are well controlled with small distortion.

The turn fault current in coil A1 when the two mitigation measures are applied is also examined in a wide operation range by varying the healthy sets currents from 20A to 120A. The resultant turn fault currents under the two mitigation methods are compared in Fig. 24. It is seen the maximum turn fault current with the current injection control is lower than that of TSC. In the light load range, the fault current under the current injection is slightly higher than that of the TSC. However, the fault current is much lower than the rated value, and it will not cause any thermal issue. It allows the machine to have larger safe margin under the worst fault scenario. The resultant torques are compared in Fig. 25 and Table IV. The output torque under current injection control is close that of the TSC when the fault turn is in coil A1. The different behaviors in the fault current and toque from those seen in Fig. 21 and Fig. 22 are caused by the differences in the injected currents as listed in Table II when the fault occurs in coil A1.
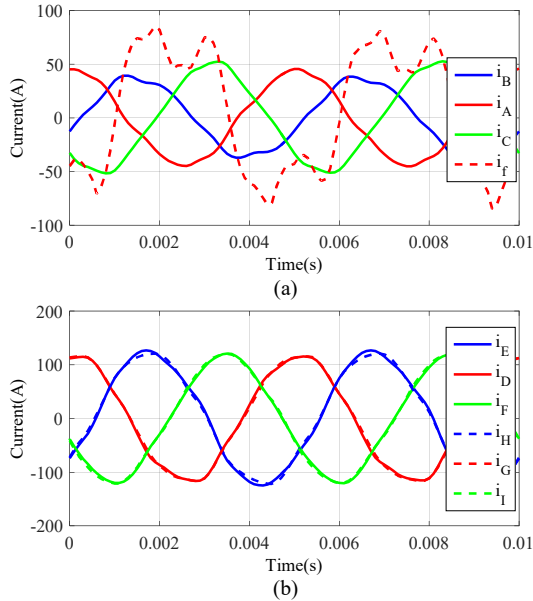

Fig. 23. Fault current and 9 phase currents (a) fault current and phase currents in set ABC (b) phase currents in healthy sets.
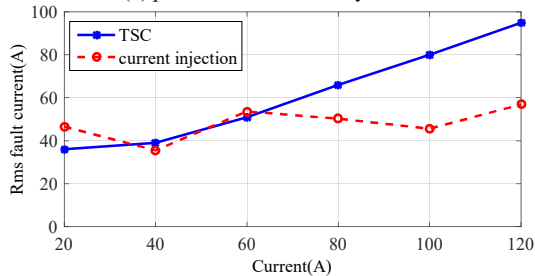

Fig. 24. Rms turn fault current variation with healthy sets currents with turn fault in coil A1 at 4000rpm.
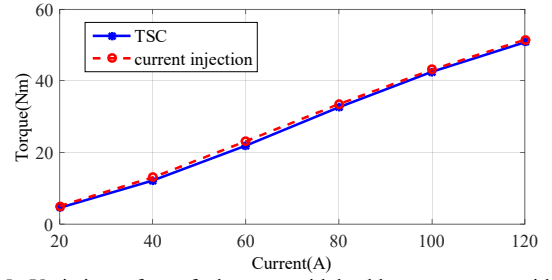

Fig. 25. Variations of post fault torque with healthy sets currents with turn fault in coil A1 at 4000rpm.

C. Integrated Fault Test with Current Injection

In practical operation, the turn fault should be timely detected and the mitigation action should be applied immediately to avoid any further damage to the machine drive. Therefore, a combined test of turn fault, fault detection and fault mitigation is performed as shown in Fig. 26. Initially, the machine is operating at 1000rpm with 60A load currents. Then, a turn fault is injected in coil B2 at 0.03s and the fault current quickly shoots to 200A. The fault is detected by the PWM ripple current based detection method in [9] and the fault phase is identified. Subsequently, the proposed current injection method is enabled to reduce the fault current. It is seen the fault current is effectively reduced to a safe level. Meanwhile the operation of the other two healthy 3-phase sets is not affected as seen from the current waveforms in Fig. 26(b). Thus, fault tolerant operation with the current injection technique is demonstrated.
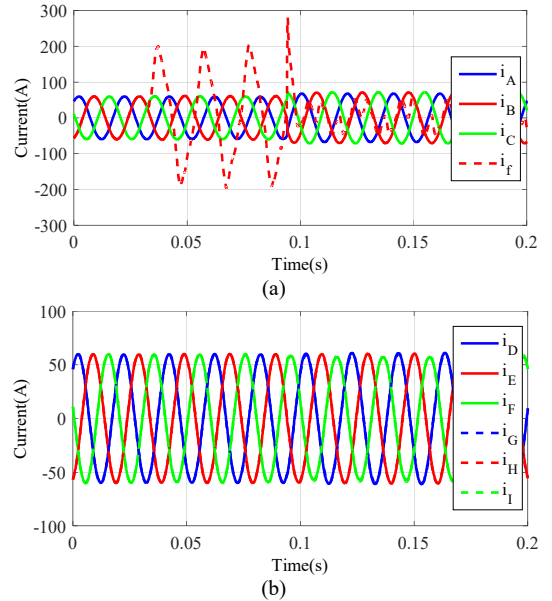
Fig. 26. Combined turn fault, detection and mitigation test (a) fault current and phase currents in set ABC (b) phase currents in healthy sets.

V. CONCLUSION

In this paper, a novel turn fault mitigation method based on current injection is proposed for the triple redundant 3x3-phase PMA SynRM. The flux linkage of the fault phase is estimated considering the influence of rotor PM and the currents in the healthy and fault 3-phase sets. This flux linkage and resultant turn fault current are minimized by injecting specific currents to the fault set while the healthy sets continue to generate torque. The proposed

approach is capable to limit the fault current for all possible turn faults scenarios, including different fault location of the sub-coils in the fault phase, different fault turn position in a slot, and different number of short-circuit turns. It has been validated by extensive FE simulations and experimental tests, demonstrating that the maximum turn fault current is effectively limited by the proposed method without compromising the torque capability compared with the conventional TSC mitigation measure.

REFERENCES

[1] S. Nadarajan, S. K. Panda, B. Bhangu, and A. K. Gupta, "Online Model-Based Condition Monitoring for Brushless Wound-Field Synchronous Generator to Detect and Diagnose Stator Windings Turn-to-Turn Shorts Using Extended Kalman Filter," *IEEE Transactions on Industrial Electronics,* vol. 63, pp. 3228-3241, 2016.

[2] B. C. Mecrow, A. G. Jack, J. A. Haylock, and J. Coles, "Fault-tolerant permanent magnet machine drives," *Electric Power Applications, IEE Proceedings -,* vol. 143, pp. 437-442, 1996.

[3] A. H. Bonnett and C. Yung, "Increased Efficiency Versus Increased Reliability," *IEEE Industry Applications Magazine,* vol. 14, pp. 29-36, 2008.

[4] S. Nandi, H. A. Toliyat, and X. Li, "Condition monitoring and fault diagnosis of electrical motors-a review," *IEEE Transactions on Energy Conversion,* vol. 20, pp. 719-729, 2005.

[5] A. Gandhi, T. Corrigan, and L. Parsa, "Recent Advances in Modeling and Online Detection of Stator Interturn Faults in Electrical Motors," *Industrial Electronics, IEEE Transactions on,* vol. 58, pp. 1564-1575, 2011.

[6] "Report of Large Motor Reliability Survey of Industrial and Commercial Installations, Part I," *Industry Applications, IEEE Transactions on,* vol. IA-21, pp. 853-864, 1985.

[7] L. Youngkook and T. G. Habetler, "An On-Line Stator Turn Fault Detection Method for Interior PM Synchronous Motor Drives," in *Applied Power Electronics Conference, APEC 2007 - Twenty Second Annual IEEE,* 2007, pp. 825-831.

[8] B. Wang, J. Wang, A. Griffo, and V. I. Patel, "Permanent Magnet Generator Turn Fault Detection Using Kalman Filter Technique," in *Energy Conversion Congress and Exposition (ECCE), 2016 IEEE,* 2016.

[9] B. Sen and J. Wang, "Stator Interturn Fault Detection in Permanent-Magnet Machines Using PWM Ripple Current Measurement," *IEEE Transactions on Industrial Electronics,* vol. 63, pp. 3148-3157, 2016.

[10] B. Sen and J. Wang, "A fast detection technique for stator inter-turn fault in multi-phase permanent magnet machines using model based approach," in *Power Electronics, Machines and Drives (PEMD 2014), 7th IET International Conference on,* 2014, pp. 1-6.

[11] B. Sen and J. Wang, "Stator inter-turn fault detection in SPM machines using PWM ripple current measurement," in *Power Electronics, Machines and Drives (PEMD 2014), 7th IET International Conference on,* 2014, pp. 1-6.

[12] A. J. Mitcham, G. Antonopoulos, and J. J. A. Cullen, "Implications of shorted turn faults in bar wound PM machines," *IEE Proceedings - Electric Power Applications,* vol. 151, pp. 651-657, 2004.

[13] B. A. Welchko, J. Wai, T. M. Jahns, and T. A. Lipo, "Magnet-flux-ing control of interior PM Machine drives for improved steady-state response to short-circuit faults," *IEEE Transactions on Industry Applications,* vol. 42, pp. 113-120, 2006.

[14] J. G. Cintron-Rivera, S. N. Foste, and E. G. Strangas, "Mitigation of Turn-to-Turn Faults in Fault Tolerant Permanent Magnet Synchronous Motors," *IEEE Transactions on Energy Conversion,* vol. 30, pp. 465-475, 2015.

[15] Y. Jiang, Z. Zhang, W. Jiang, W. Geng, and J. Huang, "Three-phase current injection method for mitigating turn-to-turn short-circuit fault in concentrated-winding permanent magnet aircraft starter generator," *IET Electric Power Applications,* vol. 12, pp. 566-574, 2018.

[16] B. Wang, J. Wang, and A. Griffo, "A Fault Tolerant Machine Drive Based on Permanent Magnet Assisted Synchronous Reluctance Machine " in *Energy Conversion Congress and Exposition (ECCE), 2016 IEEE,* Milwaukee, WI, 2016, pp. 1-8.

[17] P. Guglielmi, N. G. Giraudo, G. M. Pellegrino, and A. Vagati, "P.M. assisted synchronous reluctance drive for minimal hybrid application," in *Industry Applications Conference, 2004. 39th IAS Annual Meeting. Conference Record of the 2004 IEEE,* 2004, pp. 1-306.

[18] N. Bianchi, S. Bolognani, and M. Zigliotto, "Analysis of PM synchronous motor drive failures during flux weakening operation," in *Power Electronics Specialists Conference, 1996. PESC '96 Record., 27th Annual IEEE,* 1996, pp. 1542-1548 vol.2.

[19] B. Wang, J. Wang, A. Griffo, and B. Sen, "Experimental Assessments of a Triple Redundant 9-Phase Fault Tolerant PMA SynRM Drive," *IEEE Transactions on Industrial Electronics,* vol. 66, pp. 772 - 783, 2018.

[20] B. C. Mecrow, A. G. Jack, D. J. Atkinson, S. R. Green, G. J. Atkinson, A. King*, et al.,* "Design and testing of a four-phase fault-tolerant permanent-magnet machine for an engine fuel pump," *Energy Conversion, IEEE Transactions on,* vol. 19, pp. 671-678, 2004.

[21] Z. Sun, J. Wang, D. Howe, and G. Jewell, "Analytical Prediction of the Short-Circuit Current in Fault-Tolerant Permanent-Magnet Machines," *Industrial Electronics, IEEE Transactions on,* vol. 55, pp. 4210-4217, 2008.

[22] B. Wang, J. Wang, A. Griffo, and B. Sen, "A General Modeling Technique for a Triple Redundant 3x3-phase PMA SynRM," *IEEE Transactions on Industrial Electronics,* vol. 65, pp. 9068-9078, 2018.

[23] K. Kyung-Tae, P. Jun-Kyu, H. Jin, and K. Byeong-Woo, "Comparison of the Fault Characteristics of IPM-Type and SPM-Type BLDC Motors Under Inter-Turn Fault Conditions Using Winding Function Theory," *Industry Applications, IEEE Transactions on,* vol. 50, pp. 986-994, 2014.

[24] J. Faiz and I. Tabatabaei, "Extension of winding function theory for nonuniform air gap in electric machinery," *Magnetics, IEEE Transactions on,* vol. 38, pp. 3654-3657, 2002.

[25] J. Faiz, I. T. Ardekanei, and H. A. Toliyat, "An evaluation of inductances of a squirrel-cage induction motor under mixed eccentric conditions," *IEEE Transactions on Energy Conversion,* vol. 18, pp. 252-258, 2003.

[26] B. Sen, J. Wang, and P. Lazari, "A detailed transient model of Interior Permanent Magnet motor accounting for saturation under stator turn fault," in *Energy Conversion Congress and Exposition (ECCE), 2013 IEEE,* 2013, pp. 3548-3555.

[27] M. Dai, A. Keyhani, and T. Sebastian, "Fault analysis of a PM brushless DC Motor using finite element method," *Energy Conversion, IEEE Transactions on,* vol. 20, pp. 1-6, 2005.

[28] B. Sen and J. Wang, "Analytical modelling of stator turn fault in surface mounted permanent magnet machines," in *Energy Conversion Congress and Exposition (ECCE), 2013 IEEE,* 2013, pp. 4445-4452.

Bo Wang (M'17) received the B.Eng. and M.Sc. degrees in electrical engineering from Nanjing University of Aeronautics and Astronautics, Nanjing, China, in 2009 and 2012, respectively and the Ph.D. degree in Electronic and Electrical Engineering from the University of Sheffield, Sheffield, U.K., in 2018.

From 2012 to 2014, he served as a senior engineer in the Delta Electronics Co. Ltd. From 2017 to 2018, he was a research associate at the Department of Electronic and Electrical Engineering, University of Sheffield. Since 2018, he has joined the School of Electrical Engineering, Southeast University. His research interests include the permanent magnet machine drives, electric traction and fault tolerant systems.

Jiabin Wang (SM'03) received the B.Eng. and M.Eng. degrees from Jiangsu University, Zhengjiang, China, in 1982 and 1986, respectively, and the Ph.D. degree from the University of East London, London, U.K., in 1996, all in electrical and electronic engineering.

Currently, he is a Professor in Electrical Engineering at the University of Sheffield, Sheffield, U.K. From 1986 to 1991, he was with the Department of Electrical Engineering at Jiangsu University, where he was appointed a Lecturer in 1987 and an Associated Professor in 1990. He was a Postdoctoral Research Associate at the University of Sheffield, Sheffield, U.K., from 1996 to 1997, and a Senior Lecturer at the University of East London from 1998 to 2001. His research interests range from motion control and electromechanical energy conversion to electric drives for applications in automotive, renewable energy, household appliances and aerospace sectors.

He is a fellow of the IET and a senior member of IEEE.

Antonio Griffo (M'13) received the M.Sc. degree in electronic engineering and the Ph.D. degree in electrical engineering from the University of Napoli "Federico II," Naples, Italy, in 2003 and 2007, respectively. From 2007 to 2013, he was a Research Associate with the University of Sheffield, Sheffield, U.K., and the University of Bristol, Bristol, U.K. He is currently a Senior Lecturer with the Department of Electronic and Electrical Engineering, University of Sheffield. His research interests include modeling, control and condition monitoring of electric power systems, power electronics converters, and electrical motor drives, for renewable energy, automotive and aerospace applications.

Lei Huang(M'15) received the B.Eng. and M.Eng. degrees from China University of Petroleum(UPC), Dongying, China, in 2002 and 2008, respectively, and the Ph.D. degree from the Southeast University, Nanjing, China, in 2012, all in electrical engineering. Currently, he is an Associate Professor in Electrical Engineering at the Southeast University, Nanjing, China. He was a visiting scholar at the University of Sheffield, Sheffield, U.K., from 2017 to 2018. His research interests range from linear generators and electromechanical energy conversion to direct-drive wave energy conversion.